

Chiral magnetic textures in Ir/Fe/Co/Pt multilayers: Evolution and topological Hall signature

M. Raju^{1*}, A. Yagil^{2*}, Anjan Soumyanarayanan^{3,1}, Anthony K. C. Tan³, A. Almoalem², O. M. Auslaender^{2†}, & C. Panagopoulos^{1†}

¹*Division of Physics and Applied Physics, School of Physical and Mathematical Sciences, Nanyang Technological University, 637371 Singapore*

²*Department of Physics, Technion, Haifa 32000, Israel*

³*Data Storage Institute, Agency for Science, Technology and Research (A*STAR), 2 Fusionopolis Way, 138634 Singapore*

Skyrmions are topologically protected, two-dimensional, localized hedgehogs and whorls of spin¹. Originally invented as a concept in field theory for nuclear interactions², skyrmions are central to a wide range of phenomena in condensed matter³⁻⁵. Their realization at room temperature (RT) in magnetic multilayers⁶⁻⁸ has generated considerable interest, fueled by technological prospects and the access granted to fundamental questions. The interaction of skyrmions with charge carriers^{1,8-12} gives rise to exotic electrodynamics, such as the topological Hall effect (THE), the Hall response to an emergent magnetic field [$B_{\text{eff}}(\mathbf{r})$], a manifestation of the skyrmion Berry-phase^{13,14}. The proposal that THE can be used to detect skyrmions needs to be tested quantitatively. For that it is imperative to develop comprehensive understanding of skyrmions and other chiral textures, and their electrical fingerprint. Here, using Hall transport and magnetic imaging, we track the evolution of magnetic tex-

tures and their THE signature in a technologically viable multilayer film as a function of temperature (T) and out-of-plane applied magnetic field (H). We show that topological Hall resistivity (ρ_{TH}) scales with the density of isolated skyrmions (n_{sk}) over a wide range of T, confirming the impact of the skyrmion Berry-phase on electronic transport. We find that at higher n_{sk} skyrmions cluster into worms which carry considerable topological charge, unlike topologically-trivial spin spirals. While we establish a qualitative agreement between $\rho_{\text{TH}}(\text{H}, \text{T})$ and areal density of topological charge $n_{\text{T}}(\text{H}, \text{T})$, our detailed quantitative analysis shows a much larger ρ_{TH} than the prevailing theory predicts for observed n_{T} . Our results are pertinent for the understanding of skyrmion-THE in multilayers, where interfacial interactions, multiband transport and non-adiabatic effects play an important role, and for skyrmion applications which rely on THE. The presence of worms composed of skyrmions highlights the role of skyrmion-skyrmion interactions, which are yet to be understood.

When charge carriers flow through a conductor with their spins tracking the skyrmion spin texture, the topological Hall resistivity, ρ_{TH} , is predicted to be¹:

$$\rho_{\text{TH}} = PR'_0 n_{\text{T}} \Phi_0. \quad (1)$$

Here R'_0 is usually taken to be the ordinary Hall coefficient R_0 ^{13,15-17}, $0 < P < 1$ is the spin-polarization of the charge carriers, n_{T} the areal density of topological charge, and $B_{\text{eff}}(\mathbf{r})$ is manifested through $\Phi_0 = h/e$, the flux quantum (h is Planck's constant, $-e$ is the electron charge). Assuming skyrmions are the sole carriers of topological charge $|Q_{\text{sk}}| = 1$, n_{T} is the density of skyrmions, n_{sk} . Thus, within the adiabatic approximation, one expects a straightforward correlation between ρ_{TH} and n_{sk} . From the first observations in B20 systems^{13,14} to the recent multilayers,

THE has been used as an indicator for the presence of skyrmions^{8,15}. However, a clear understanding of the effect is still lacking¹⁸, especially in technologically viable multilayer films^{8,16,17}, where disorder and interface effects can play an important role^{7,19,20}.

Using magnetic force microscopy (MFM) and transport measurements we present a comprehensive picture of the evolution of magnetic textures and their THE signature in a multilayer film capable of hosting skyrmions from RT down to at least 5 K. We demonstrate the relationship between n_{sk} and $|\rho_{\text{TH}}|$ over a ≈ 200 K temperature (T) range. As the applied field H is swept towards zero, we find that skyrmions aggregate in worm-like magnetic textures, which carry a large topological charge, and manifest as peaks in ρ_{TH} . Quantitative modeling of these worm-textures uncovers qualitative agreement between $\rho_{\text{TH}}(H, T)$ and $n_{\text{T}}(H, T)$. Despite this, we find a large quantitative discrepancy indicating that the effect in multilayers is more involved.

Here we use sputtered $[\text{Ir}(1)/\text{Fe}(0.5)/\text{Co}(0.5)/\text{Pt}(1)]_{20}$ (in parenthesis – thickness in nanometers) multilayer films, with the composition chosen for exhibiting skyrmions across a large range of T . The RT characterization of the films through magnetization, MFM and micromagnetic simulations indicated the key magnetic parameters responsible for skyrmion formation, Dzyaloshinskii-Moriya interaction (DMI, D), and exchange interaction (A) to be $D \approx 2.0$ mJ/m², $A \approx 11$ pJ/m⁸. The effective anisotropy (K_{eff}) varies in the range ≈ 0.2 – 0.01 MJ/m³ as we change T from 5 K to 300 K²¹. As demonstrated here, control over skyrmion density through variation of T is the key for unambiguous verification of the skyrmion THE signature. In contrast to the B20 compounds, which host lattices of tubular Bloch-skyrmions²², multilayers sustain skyrmions with tun-

able diverse properties, and offer smoother integration with existing spintronic technologies. Spin textures in multilayers are influenced by interlayer dipolar and exchange interactions, magnetic frustration²³, and granularity⁷, which can pin, stabilize, and deform the spin textures, and result in coupled pancake-skyrmions with different topologies^{20,23}. This complexity, and associated tunability, provide means for exploring the interplay between disorder, interactions, and topology.

The magnetoresistance and Hall effect were measured using a lock-in with non-perturbative current densities ($\approx 10^5$ A/m²). The presence of skyrmions is associated with an additional component in the measured Hall signal (ρ_{yx})¹³⁻¹⁵. This contribution can be quantified by resolving ρ_{yx} into the ordinary (R_0H) and anomalous [$R_S M(H)$] Hall components, and an extra component (ρ_{TH})^{13,15-17}:

$$\rho_{yx}(H) = R_0H + R_S M(H) + \rho_{TH}(H). \quad (2)$$

We estimate $\rho_{TH}(H)$ by $\Delta\rho_{yx}(H)$, the residual of the fit of $\rho_{yx}(H)$ to $\rho_{yx}^{fit}(H) = R_0H + R_S M(H)$, which also yields R_0 and R_S ²¹. The accuracy of $\Delta\rho_{yx}$ is ensured by calibrating field offsets to avoid artifacts resulting from using different measurement set-ups²¹. Our conservative estimate for the overall error in $\Delta\rho_{yx}$, including a contribution from data analysis, is ± 2 n $\Omega \cdot$ cm, corresponding to the non-zero residual signal beyond saturation, where there are no skyrmions. Figure 1(a) shows $\Delta\rho_{yx}(H)$ at 5 K, with the overall features persisting to at least 300 K⁸.

For MFM we followed the same field sweep from saturation as we did for $\rho_{yx}(H)$ and $M(H)$ – the images were acquired at field increments as H was swept²¹. Figure 1(b)-(k) shows the result for 5 K. Overall, we observe a similar evolution of the magnetic textures at

$T = 50, 100, 150, 200 \text{ K}^{21}$.

We begin by comparing the magnetic textures to $\Delta\rho_{yx}(H)$. Beyond saturation MFM shows the null signal expected for a polarized ferromagnet²¹. This corresponds to suppressed $\Delta\rho_{yx}$ [Fig. 1(a)], indicating the topologically trivial nature of the polarized state. The onset of $\Delta\rho_{yx}$ commences at $\mu_0 H \approx -0.3 \text{ T}$ with the nucleation of sub-100 nm magnetic domains, indicating the emergence of a finite Berry-phase resulting from nontrivial topology [Fig. 1(b)], which we identify as Néel-skyrmions¹⁹. By $\mu_0 H \approx -0.25 \text{ T}$ [Fig. 1(c)] the increasing n_{sk} corresponds to a substantial $\Delta\rho_{yx}$ as expected from $|\rho_{\text{TH}}| \propto n_{\text{sk}}^1$. Also, as n_{sk} increases, skyrmions aggregate to form worm-like features [Fig. 1(c)]. By $\mu_0 H \approx -0.225 \text{ T}$, images show only worms [Fig. 1(d),(e)]. Surprisingly, at this field $\Delta\rho_{yx}$ peaks, indicating a significant contribution from the worms which therefore must have nontrivial topology. Meanwhile, the dense textures at intermediate H , [Fig. 1(f)-(h),²¹], correspond to reduced, yet finite, $\Delta\rho_{yx}$. Careful inspection of such scans also reveals worm-like features²¹, to which we attribute the finite magnitude of $\Delta\rho_{yx}$.

As $H = 0$ is approached, the worms evolve into labyrinthine helical stripes, and proliferate at the expense of the polarized background. This is coincident with a suppression of $\Delta\rho_{yx}$, highlighting the close relationship between $\Delta\rho_{yx}$ and the magnetic texture. As H is increased towards positive saturation, the labyrinthine stripes evolve into worms, skyrmions, and eventually a uniformly polarized phase [Fig. 1(i)-(k)]. As expected for a texture with an opposite topological charge, the sign of $\Delta\rho_{yx}$ is reversed when $H > 0$. However, the MFM contrast does not change, due to reversal of the tip magnetization near 0.1 T.

The distinct field ranges for isolated skyrmions (near saturation), worms (negative peak in $\Delta\rho_{yx}$) and their coexistence (positive peak in $\Delta\rho_{yx}$) offer a unique opportunity to compare the magnetic texture with $\Delta\rho_{yx}$. In particular: (i) Does $\Delta\rho_{yx}$ track n_{sk} ? (ii) How do worms produce such a large $\Delta\rho_{yx}$? (iii) Is there quantitative consistency between $\Delta\rho_{yx}$ and n_{T} ?

To address (i) we exploit $n_{\text{sk}}(T)$, which increases by an order-of-magnitude when we increase T from 5 K to 200 K (Fig. 2). We attribute this proliferation to the suppression of the critical DMI $D_{\text{C}} = 4(AK_{\text{eff}})^{1/2}/\pi$ as K_{eff} decreases⁸. Interestingly, skyrmion size is only weakly dependent on T , not unlike theoretical predictions²⁴. Importantly, we find that $\Delta\rho_{yx}(T)$ tracks $n_{\text{sk}}(T)$ over the entire range [Fig. 2(a)]. This verification of $|\rho_{\text{TH}}| \propto n_{\text{sk}}$ was not possible previously due to limited tunability of n_{sk} in skyrmion systems reported so far. This validates the topologically non-trivial nature of the skyrmions and the viability of our approach.

Having established the direct correspondence between n_{sk} and $\Delta\rho_{yx}$, we now examine the worms. Though the presence of worms is expected in systems with competing interactions, such as in ferromagnetic films²⁵, their topological role is not obvious. In recent MFM work on Bloch skyrmions in a B20 compound²², helical stripe domains resulting from merging skyrmions were assigned $|Q_{\text{W}}| = 1$ – each stripe was described by two half-skyrmions connected by a topologically trivial straight domain²². This motivates the examination of whether worms carrying a topological charge $|Q_{\text{W}}| = 1$ can describe our results. We therefore plot $n_{\text{sk}} + n_{\text{w}}$ (n_{w} is the number of worms per unit area) in Fig. 3(a), with the sign chosen from the sign of $\Delta\rho_{yx}$. As the plot shows, both $n_{\text{sk}}(H)$ and $n_{\text{sk}}(H) + n_{\text{w}}(H)$ do not track $\Delta\rho_{yx}(H)$. This calls for a closer look at the topological

nature of the worms.

The following analysis is motivated by sequences like Fig. 1(b)-(d), which suggest that worms result from skyrmions clustering as n_{sk} increases. The transition of worms into typical stripe domains with $|Q_{\text{W}}| = 1$ requires a complete unwinding of their internal spin structure. The energy barrier for this suggests that the effective topological charge should be at least equal to the total number of skyrmions that form a worm (i.e. $|Q_{\text{W}}| > 1$). While skyrmions are expected to repel each other on very short length-scales because of exchange coupling²⁶, clusters can be stabilized by attraction on an intermediate scale, due to exchange frustration²⁷.

Here our recent work, a magnetic multipole expansion of the field from skyrmions (MEFS)¹⁹, provides a direct method to associate an effective Q_{W} with each worm. Figures 3(b)-(g) show two typical examples where we fit the measured signal from worms by trains of skyrmions. Such images, which contain both skyrmions and worms, provide the foundation for this kind of analysis – the isolated skyrmions serve to constrain the fit amplitude per skyrmion, and improve the accuracy²¹. Meanwhile, the analysis of images containing only worms [Fig. 1(d)] hinges on skyrmions-skyrmion repulsion on a length scale comparable to their radius²⁶. Therefore, the number of skyrmions clustered in a worm is determined by the total length of the worm, and the typical radius of skyrmions [≈ 40 nm¹⁹]. For images with densely packed features [e.g. Figs. 1(f)-(h)] identifying and extracting the worms themselves requires additional image processing, for which we employ a deep-learning-model-based algorithm, which extracts features relevant for classification from supplied examples²¹.

The qualitative match between $n_T(H)$ estimated from $\sum Q_W + \sum Q_{sk}$ and $\Delta\rho_{yx}(H)$ [Fig. 3(a)] reinforces our modeling of worms as trains of skyrmions and confirms that $\Delta\rho_{yx} \approx \rho_{TH}$, and with it the topological nature of the worms. Our observations on the emergence of worms with a high topological number, previously not noticed experimentally, indicate they are distinct from trivial spin spirals, and form an essential part of the phase diagram for multilayer skyrmions²⁸. The presence of worms in a tunable multilayer offers a platform for studying skyrmion-skyrmion interactions over a wide parameter range, as well as applications, such as skyrmion racetracks⁷.

Having established the nontrivial topology of the worms and a qualitative match between $\rho_{TH}(H, T)$ and $n_T(H, T)$, we examine the quantitative match. As we show in Fig. 3(a), the density of topological charge estimated from THE [$\Delta\rho_{yx}/(PR_0\Phi_0)$, Eq. 1] indicates a two-orders-of-magnitude discrepancy. This implies that the assumptions invoked in using Eq. 1 to understand the topological signatures of chiral magnetic textures in multilayer skyrmion-hosts, are insufficient for a comprehensive description of the measured $\Delta\rho_{yx}$.

A possible culprit is the assignment $R'_0 = R_0$ in Eq. 1²⁹, justified for a single band material. This is not the case here: Bulk Fe and Co, the ferromagnetic ingredients of our multilayer stack, have several active electron and hole bands³⁰. In such materials R_0 is suppressed because electrons and holes, which experience the same H , compensate each other's contributions. The cancellation estimated from values reported for bulk Fe³⁰ indicate suppression of R_0 by an order of magnitude from the separate contributions of individual bands, partially addressing the discrepancy²¹. Importantly, the cancellation may not happen in the same way for B_{eff} – the Berry-phase can act

differently on charge carriers from different bands³¹, with an associated sensitivity to occupation³². The fact that the peak value of $\Delta\rho_{yx}(H)$ changes by only $\approx 25\%$ with T despite the sign change of $R_0(T)$ [Fig. 2(b)], probably because of small variations of the occupations of the compensating bands, further confirms that $R'_0 \neq R_0$. In this case, using R_0 in Eq. 1 underestimates ρ_{TH} ^{16,17}, although once R'_0 is determined this fundamental equation may still be used. For this it is essential to account for the electronic band structure of the chiral magnet.

Our complementary imaging and electrical transport studies elucidate the complexity of the Berry-phase associated with the electrical fingerprint of chiral magnetic textures in technologically viable magnetic multilayers. For a comprehensive understanding and in order to utilize THE emerging from magnetic skyrmions, it is imperative to consider (a) the band structure contributing to THE, (b) the possibility of $|Q_{\text{sk}}| > 1$ ²³, (c) the coupling of skyrmions across layers and complex magnetic textures in buried interfaces²⁰, (d) the contribution from topologically trivial chiral configurations driven by magnetic spin-frustration¹⁸, and (e) the validity of the commonly assumed adiabatic approximation¹⁸.

Acknowledgements It is our pleasure to thank A. Petrović for inputs on transport experiments, as well as D. Arovas, A. Auerbach, Shi-Zeng Lin, D. Podolsky, M. Reznikov, and A. Turner for illuminating discussions. We also thank G. Goldman and Y. Schechner for help with image analysis. The work in Singapore was supported by the Ministry of Education (MoE) – Academic Research Fund (Ref. No. MOE2014-T2-1-050), the National Research Foundation – NRF Investigatorship (Reference No. NRF-NRFI2015-04), and the A*STAR Pharos Fund (1527400026). Work at Technion was supported by the Israel Science Foundation (Grant no. 1897/14). We would also like to thank the Micro Nano Fabrication Unit, and to acknowledge

support from the Russell Berrie Nano Technology Institute, both at the Technion.

Contributions MR, AS, OMA, and CP designed and initiated the research. MR deposited the films and characterized them with AS and AT. MR performed and analyzed magnetization and transport measurements with inputs from AS, OMA, and CP. AY performed the low temperature MFM experiments with assistance from AA, and AY and OMA analyzed the low temperature MFM data. OMA and CP coordinated the project. All authors discussed the results and provided inputs to the manuscript.

***These authors are equal contributors**

Competing Interests The authors declare that they have no competing financial interests.

†Correspondence Correspondence and requests for materials should be addressed to to:
ophir@physics.technion.ac.il / christos@ntu.edu.sg.

References

1. Nagaosa, N. & Tokura, Y. Topological properties and dynamics of magnetic skyrmions. *Nat. Nano.* **8**, 899–911 (2013).
2. Skyrme, T. H. R. A non-linear field theory. *Proc. R. Soc. Lond. A* **260**, 127–138 (1961). URL <http://rspa.royalsocietypublishing.org/content/260/1300/127>.
3. Sondhi, S. L., Karlhede, A., Kivelson, S. A. & Rezayi, E. H. Skyrmions and the crossover from the integer to fractional quantum Hall effect at small Zeeman energies. *Phys. Rev. B*

- 47, 16419–16426 (1993). URL <http://link.aps.org/doi/10.1103/PhysRevB.47.16419>.
4. Senthil, T., Vishwanath, A., Balents, L., Sachdev, S. & Fisher, M. P. A. Deconfined quantum critical points. *Science* **303**, 1490–1494 (2004). URL <http://science.sciencemag.org/content/303/5663/1490>.
 5. Wang, F., Kivelson, S. A. & Lee, D.-H. Nematicity and quantum paramagnetism in FeSe. *Nat. Phys.* **11**, 959–963 (2015). URL <http://www.nature.com/doi/10.1038/nphys3456>.
 6. Moreau-Luchaire, C. *et al.* Additive interfacial chiral interaction in multilayers for stabilization of small individual skyrmions at room temperature. *Nat. Nano.* **11**, 444–448 (2016).
 7. Woo, S. *et al.* Observation of room-temperature magnetic skyrmions and their current-driven dynamics in ultrathin metallic ferromagnets. *Nat. Mater.* **15**, 501–506 (2016). URL <http://www.nature.com/nmat/journal/vaop/ncurrent/full/nmat4593.html>.
 8. Soumyanarayanan, A. *et al.* Tunable room-temperature magnetic skyrmions in Ir/Fe/Co/Pt multilayers. *Nat. Mater.* **16**, 898 (2017). URL <https://www.nature.com/nmat/journal/vaop/ncurrent/full/nmat4934.html>.
 9. Bogdanov, A. N. & Röbber, U. K. Chiral symmetry breaking in magnetic thin films and multilayers. *Phys. Rev. Lett.* **87**, 037203 (2001).
 10. Soumyanarayanan, A., Reyren, N., Fert, A. & Panagopoulos, C. Emergent phenomena induced by spin-orbit coupling at surfaces and interfaces. *Nature* **539**, 509–517 (2016).

11. Jiang, W. *et al.* Direct observation of the skyrmion Hall effect. *Nat. Phys.* **13**, 162–169 (2016).
URL <http://www.nature.com/doi/10.1038/nphys3883>.
12. Litzius, K. *et al.* Skyrmion Hall effect revealed by direct time-resolved X-ray microscopy. *Nat. Phys.* **13**, 170–175 (2017). URL <http://www.nature.com/nphys/journal/v13/n2/full/nphys4000.html>.
13. Neubauer, A. *et al.* Topological Hall effect in the A phase of MnSi. *Phys. Rev. Lett.* **102**, 186602 (2009). URL <http://link.aps.org/doi/10.1103/PhysRevLett.102.186602>. Erratum *Phys. Rev. Lett.* **110**, 209902 (2013).
14. Lee, M., Kang, W., Onose, Y., Tokura, Y. & Ong, N. P. Unusual hall effect anomaly in MnSi under pressure. *Phys. Rev. Lett.* **102**, 186601 (2009). URL <http://link.aps.org/doi/10.1103/PhysRevLett.102.186601>.
15. Matsuno, J. *et al.* Interface-driven topological hall effect in SrRuO₃ – SrIrO₃ bilayer. *Sci. Adv.* **2**, e1600304 (2016).
16. Maccariello, D. *et al.* Electrical detection of single magnetic skyrmions in metallic multilayers at room temperature. *Nat. Nanotechnol. (online)* (2018). URL <http://www.nature.com/articles/s41565-017-0044-4>.
17. Zeissler, K. *et al.* Direct imaging and electrical detection at room temperature of a single skyrmion. *arXiv:1706.06024* (2017). URL <https://arxiv.org/abs/1706.06024>.

18. Denisov, K. S., Rozhansky, I. V., Averkiev, N. S. & Lähderanta, E. A nontrivial crossover in topological Hall effect regimes. *Sci. Rep.* **7**, 17204 (2017). URL <http://www.nature.com/articles/s41598-017-16538-4>.
19. Yagil, A. *et al.* Stray field signatures of Néel textured skyrmions in Ir/Fe/Co/Pt multilayer films. *arXiv:1705.07608* (2017). URL <http://arxiv.org/abs/1705.07608>.
20. Legrand, W. *et al.* Hybrid chiral domain walls and skyrmions in magnetic multilayers. *arXiv:1712.05978* (2017). URL <http://arxiv.org/abs/1712.05978>.
21. See Supplementary Information.
22. Milde, P. *et al.* Unwinding of a skyrmion lattice by magnetic monopoles. *Science* **340**, 1076–1080 (2013). URL <http://www.sciencemag.org/content/340/6136/1076>.
23. Rózsa, L. *et al.* Formation and stability of metastable skyrmionic spin structures with various topologies in an ultrathin film. *Phys. Rev. B* **95**, 094423 (2017). URL <https://link.aps.org/doi/10.1103/PhysRevB.95.094423>.
24. Tomasello, R. *et al.* Origin of temperature and field dependence of magnetic skyrmion size in ultrathin nanodots. *arXiv:1706.07569* (2017). URL <http://arxiv.org/abs/1706.07569>.
25. Seul, M. & Andelman, D. Domain shapes and patterns: The phenomenology of modulated phases. *Science* **267**, 476–483 (1995). URL <http://science.sciencemag.org/content/267/5197/476>.

26. Shi-Zeng Lin, Reichhardt, C., Batista, C. D. & Saxena, A. Particle model for skyrmions in metallic chiral magnets: Dynamics, pinning, and creep. *Phys. Rev. B* **87**, 214419 (2013). URL <http://link.aps.org/doi/10.1103/PhysRevB.87.214419>.
27. Rózsa, L. *et al.* Skyrmions with attractive interactions in an ultrathin magnetic film. *Phys. Rev. Lett.* **117**, 157205 (2016). URL <https://link.aps.org/doi/10.1103/PhysRevLett.117.157205>.
28. Dupé, B., Hoffmann, M., Paillard, C. & Heinze, S. Tailoring magnetic skyrmions in ultra-thin transition metal films. *Nat. Commun.* **5**, 4030 (2014). URL <http://www.nature.com/ncomms/2014/140604/ncomms5030/full/ncomms5030.html>.
29. Onoda, M., Tatara, G. & Nagaosa, N. Anomalous Hall effect and skyrmion number in real and momentum spaces. *J. Phys. Soc. Jpn.* **73**, 2624–2627 (2004). URL <http://journals.jps.jp/doi/abs/10.1143/JPSJ.73.2624>.
30. Pugh, E. M. & Rostoker, N. Hall effect in ferromagnetic materials. *Rev. Mod. Phys.* **25**, 151–157 (1953). URL <https://link.aps.org/doi/10.1103/RevModPhys.25.151>.
31. Ritz, R. *et al.* Giant generic topological Hall resistivity of MnSi under pressure. *Phys. Rev. B* **87**, 134424 (2013). URL <https://link.aps.org/doi/10.1103/PhysRevB.87.134424>.
32. Göbel, B., Mook, A., Henk, J. & Mertig, I. Unconventional topological Hall effect in skyrmion crystals caused by the topology of the lattice. *Phys. Rev. B* **95**, 094413 (2017). URL <https://link.aps.org/doi/10.1103/PhysRevB.95.094413>.

33. Rajanikanth, A., Kasai, S., Ohshima, N. & Hono, K. Spin polarization of currents in Co/Pt multilayer and CoPt alloy thin films. *Appl. Phys. Lett.* **97**, 022505 (2010). URL <http://aip.scitation.org/doi/10.1063/1.3460910>.

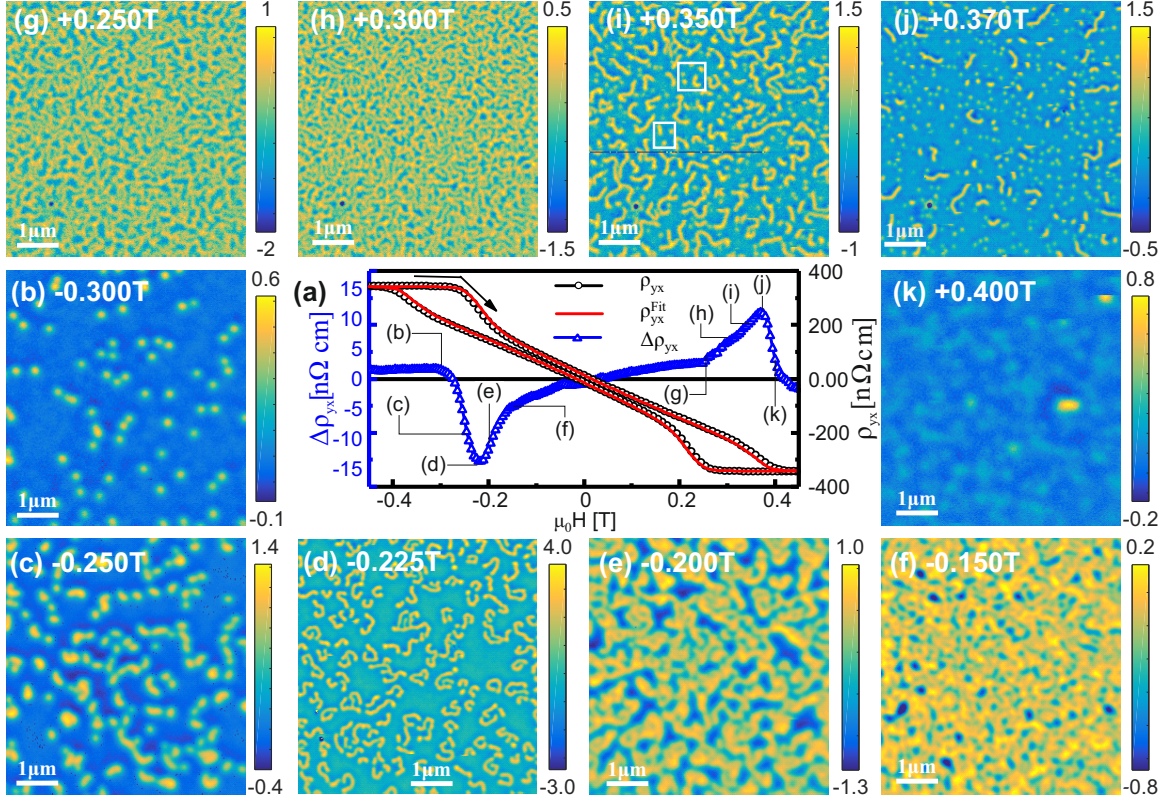


Figure 1: Evolution of magnetic textures and THE with H at $T = 5$ K. **(a)** $\rho_{yx}(H)$, $\rho_{yx}^{fit}(H)$ and the residual $\Delta\rho_{yx}(H) = \rho_{yx}(H) - \rho_{yx}^{fit}(H) \approx \rho_{TH}(H)$. Black arrow indicates field sweep direction for $\Delta\rho_{yx}$ and MFM, while ρ_{yx} and ρ_{yx}^{fit} are shown for both sweep directions. **(b)-(k)** Selected MFM scans [full sequence in²¹, scan-height $h = 75, 60, 40, 60, 65, 50, 60, 50, 45, 60$ nm for each of (b)-(k); color bars give Δf range.] Frames in (i) mark features in focus in Fig. 3(b)-(g).

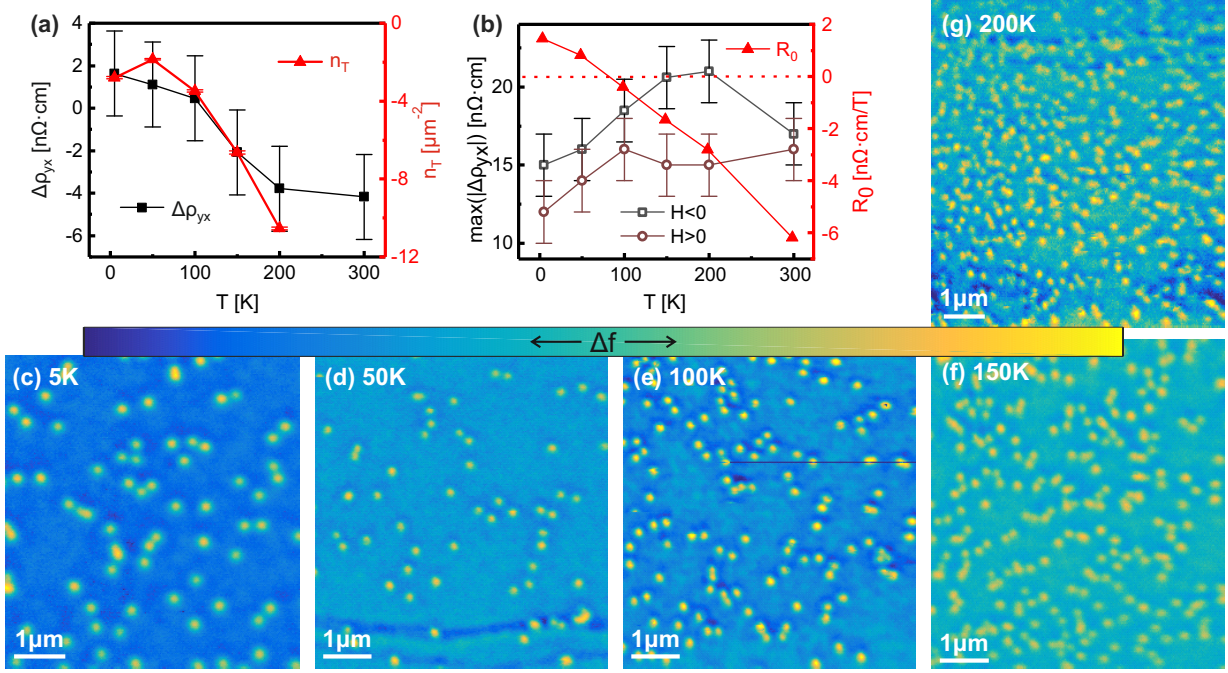


Figure 2: Temperature dependence of n_T , $\Delta\rho_{yx}$, and R_0 . **(a)** $\Delta\rho_{yx}(T)$ (left axis, squares) compared with topological charge $|n_T(T)| = n_{sk}(T)$ (right axis, triangles) at -0.3 T, corresponding to the isolated skyrmions in (c)-(g). The error bars for $\Delta\rho_{yx}$ represent a conservative estimate of the systematic error. **(b)** Left axis: Magnitude of the THE peaks ($H < 0$ – squares, $H > 0$ – circles). Right axis: The fit parameter $R_0(T)$ from Eq. 2 (triangles). **(c)-(g)** MFM scans showing isolated skyrmions for $n_T(T)$ in (a). [For (c)-(g) scan-height $h = 75, 40, 40, 100, 40$ nm, $\Delta f_{\text{range}} = 0.7, 6, 4, 1.8, 2$ Hz. (c) is Fig. 1(b).]

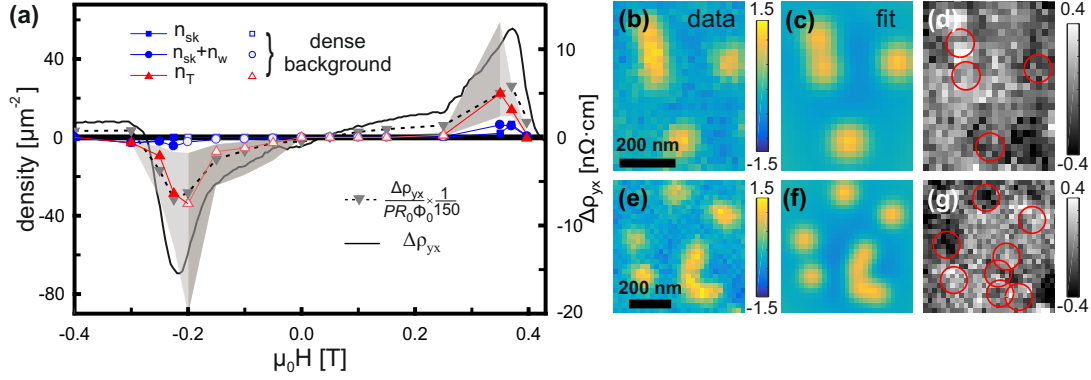


Figure 3: Comparison between $\Delta\rho_{yx}$ and the signed density of topological charge at 5 K. **(a)** Right axis: $\Delta\rho_{yx}$ (solid line). Left axis: n_{sk} (squares), $n_{\text{sk}} + n_{\text{w}}$ (circles), n_{T} (triangles), and $\Delta\rho_{yx}/(PR_0\Phi_0)$ (cf. Eq. 1, inverted triangles with dotted line) using $P = 0.56^{33}$ and R_0 from Fig. 2(b). For n_{T} , each worm is assigned several skyrmions $|Q_{\text{W}}|$ by fit [cf. (b)-(g)], and each isolated skyrmion is counted once. Empty symbols indicate points with a lower confidence, that result from counting worms in a dense background²¹. Shaded area shows confidence bounds for n_{T} resulting from fit details discussed in²¹. **(b),(e)** Zooms on areas in Fig. 1(i) with skyrmions and isolated worms. **(c),(f)** Results of MEFS fits wherein all skyrmions, including those assigned to worms, are treated as identical. The fit peak height ≈ 1.15 Hz, full width at half maximum (FWHM) ≈ 100 nm, and $|Q_{\text{W}}| = 2$ in (c) and $|Q_{\text{W}}| = 4$ in (f).] **(d),(g)** Difference plots between (b) and (c), and between (e) and (f), showing the quality of the fit. Circles give the locations of the skyrmions in the fit. [Color bars give Δf_{range} .]